Journal of Structural Geology, Vol. 8, No. 5, pp. 517 to 526, 1986
Printed in Great Britain

0191-8141/86 $3.00+0.00
Pergamon Journals Ltd.

A spherical electron-channelling pattern map for use in quartz petrofabric analysis

GEOFFREY E. LLOYD*

Department of Metallurgy and Materials, University of Birmingham, Birmingham B15 2TT, U.K.

and

COLIN C. FERGUSON†

Kansas Geological Survey, University of Kansas, Lawrence, KS 66044, U.S.A.

(*Received* 5 *February* 1985; *accepted in revised form* 20 *June* 1985)

Abstract—Electron channelling patterns (ECP's) are formed in the scanning electron microscope (SEM) by the interaction between the incident electrons and the lattice of crystalline specimens. The patterns are unique for a particular crystallographic orientation and are therefore of considerable potential in petrofabric studies provided they can be accurately indexed. Indexing requires an ECP-map of the crystallographic stereogram or unit triangle covering all possible orientations and hence ECP patterns. Due to the presence of long-range distortions in planar ECP-maps, it is more convenient to construct the maps over a spherical surface. This also facilitates the indexing of individual ECP's. A spherical ECP-map for quartz is presented together with an example of its use in petrofabric analysis.

INTRODUCTION

THE DETERMINATION of crystallographic fabric is often central to microstructural interpretation of deformed rocks. Traditionally, the petrographic microscope incorporating a universal stage has been used to provide this information but X-ray diffraction (XRD) and transmission electron microscope (TEM) techniques have become increasingly popular. These approaches all have their limitations. Universal-stage methods, although discriminating between individual grains, are laborious and are restricted to a few specific orientations. XRD techniques are indiscriminate and hence can only provide bulk crystallographic information, although most orientations are amenable to analysis. The TEM is restricted to very small regions of thin foils and consequently the images are often very difficult to relate to observations made on the thin-section and hand-specimen scales. Thus there is a need for a discriminatory technique which is capable of providing accurate crystallographic information on any orientation for different minerals in representative specimens. The scanning electron microscope (SEM) affords such a facility in its electron-channelling mode of operation.

It has been known for some time (e.g. Holt *et al.* 1974, Goldstein & Yakowitz 1975) that backscattered primary electrons (BSE's) contain information on both phase distribution (atomic number contrast) and crystallography (electron channelling contrast). This paper is concerned only with electron channelling contrast which is caused by the interaction between primary electrons and the crystallographic structure of the target specimen. Two types of image may be obtained: (a) orientation contrast, in which regions of constant orientation appear as uniform contrast (Fig. 1a) and (b) electron channelling patterns (ECP's), distinct configurations of lines and bands of differing contrast (Fig. 1b) which are unique for a particular orientation. The basic principles of SEM electron-channelling contrast have been described by Joy (1974), Goldstein & Yakowitz (1975), Schulson (1977) and Hall & Hutchinson (1980), while Lloyd & Hall (1981) and Lloyd *et al.* (1981) discussed geological considerations (see also Saimoto *et al.* 1980).

Orientation contrast and ECP images result from the channelling of the incident electrons through the structure of crystalline specimens and arise because of the different atomic packing densities in the various crystallographic directions. For some incidence angles of the primary electron beam the packing is relatively dense and electrons tend to interact with the specimen close to the surface, but for other angles the packing is less dense and the electrons are able to penetrate or channel farther into the specimen (Hirsch *et al.* 1962, Booker *et al.* 1967). Since the probability of emission of BSE's decreases with penetration, deeply channelled electrons are less likely to escape than those which interact close to the specimen surface. Electron channelling is therefore restricted to within approximately 50 nm of the specimen surface. The behaviour of the electrons inside the specimen can be described in terms of the superposition of plane or *Bloch* waves modulated by the periodic potential of the crystal structure. These waves are solutions of the Schrödinger Equation and represent physi-

* Present address: Department of Earth Sciences, The University, Leeds, LS2 9JT, U.K.
† Present address: Department of Geology, Birkbeck College, University of London, London W1P 1PA, U.K.

cally the current flows within the structure. The relative contributions of each wave to the overall BSE signal varies with the angle between the incident electron beam and the different structure planes according to the Bragg Law and this ultimately determines the level of contrast observed in the electron channelling image. In general, if the incident beam scans at low magnification over a region of constant orientation an ECP is likely to be observed, but if the magnification is high and/or the area scanned is large compared to the regions of constant orientation, an orientation contrast image is more likely. However it is possible to switch from one image to the other so that, used in combination, these two SEM imaging techniques permit individual grains (or subgrains) of >10 μm diameter to be discerned and accurately indexed provided the relevant ECP-map is available for identification purposes.

ECP-maps (e.g. Joy 1974) consist of individual ECP's joined together to cover the whole of the crystallographic stereogram or unit triangle required by symmetry to represent all possible orientations (e.g. Fig. 2a). In principle, each mineral requires its own map, but in practice it may be sufficient to use a map of the same crystal symmetry class, although large variations in the number of ions present in the unit cell can lead to difficulties in pattern recognition. ECP-maps are already available for high symmetry classes, such as face-centred and body-centred cubic (e.g. Joy 1974, Lloyd *et al.* 1981), but none exist for the geologically important low symmetry classes. In this contribution we present an ECP-map for trigonal symmetry suitable for use in quartz petrofabric studies.

CONSTRUCTION OF ECP-MAPS

ECP-maps are ideally constructed by joining together a number of individual ECP's obtained from a single crystal as it is progressively tilted with respect to the incident electron beam such that its crystallographic orientation apparently changes (e.g. Joy 1974). Using the SEM/BSE operating configuration described by Lloyd *et al.* (1981) the individual channelling patterns represent the orientation of the grain-normal direction with respect to the specimen surface. Since the ECP's are recorded photographically, the camera length remains constant for all orientations irrespective of specimen tilt and so the composite map is effectively created over the surface of a sphere. Therefore any attempt to construct a planar ECP-map inevitably involves distortions resulting in errors in both beam and orthogonal reference directions. Stott *et al.* (1975) reported that for cubic symmetry maps the former error is probably $<3°$ but the latter error may be as great as 15° due to the large extrapolations involved. It is possible to accommodate these distortions in planar ECP-maps for materials with high crystal symmetry by varying size of the photographic print with the distance from the centre of the projection (e.g. Fig. 2a); but as the symmetry decreases, the size of the unit triangle and hence the ECP-map increases, leading to more serious distortions and errors which cannot be accommodated photographically.

Because all ECP-maps are generated over a spherical surface the most accurate method of constructing a distortion-free map is to use a sphere. This approach was first demonstrated by Stott *et al.* (1975) using a 36.55 cm diameter metal globe and ECP prints adjusted to coincide with this diameter (e.g. Fig. 2b). Since the constituent ECP's typically extend over $<20°$, the local deviation from sphericity is small and hence no long-range distortion develops (although minor distortions do occur at the periphery of the patterns such that it is usually advisable to include only the central portion of any ECP). An advantage of spherical ECP-maps is that they accurately reflect the real nature of crystallographic orientations. Individual ECP's can therefore be represented directly by three spherical Euler angles (e.g. Roe 1965, Williams 1968, Bunge & Wenk 1977) which locate the position of the pattern with respect to the crystallographic and specimen reference frames. The Euler angles are measured using curved metal rulers (Fig. 2b) and correspond directly to the three orthogonal axes of orientation space. It is therefore a relatively simple matter to construct orientation distribution function (ODF) diagrams from ECP's. Furthermore, pole figures and inverse pole figures can be derived from these angles using a straightforward transformation matrix (Roe 1965).

A much simpler, but nevertheless accurate, method of representing ECP's also exists. The positions of the pattern centres are marked on an overlay of the ECP-map. This is an easy matter for planar maps, but is more difficult for spherical maps, where it is still necessary to fix the pattern-normal by two spherical angles. This approach considers the ECP (or grain) normals in terms of crystal coordinates and hence produces an inverse pole figure type of fabric diagram.

Although for high crystal symmetry classes spherical ECP-maps can be constructed from a single specimen merely by tilting, it is impossible to tilt specimens with low symmetry sufficiently in the SEM to cover the whole unit triangle. Thus several specimens cut at different orientations from a single crystal are required, from which partial ECP-maps can be obtained and then merged together over a spherical surface. This approach is necessary for the construction of any map based on quartz.

SPHERICAL ECP-MAP FOR QUARTZ

Quartz crystallography

Quartz crystallizes in the trigonal symmetry system, trapezohedral class (32), and consequently has a large unit triangle. Fabric analyses with the X-ray texture goniometer generally assume a 60° unit triangle inverse pole figure with corners at *m*, *c* and *m* forms and

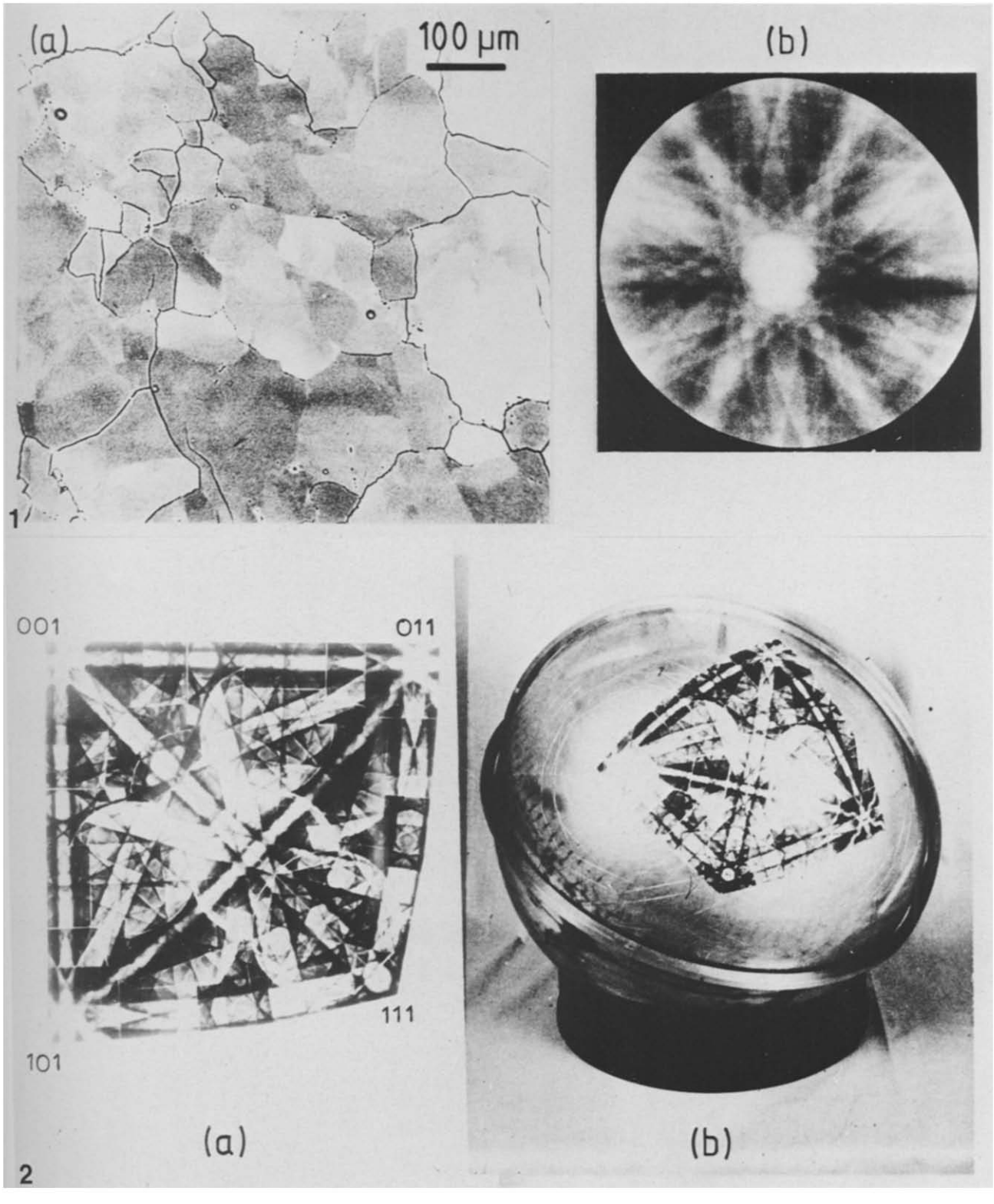

Fig. 1. Examples of the two types of electron-channelling contrast image obtained from backscattered electrons in the SEM. Specimen is a deformed quartzite from Tongue, N. Scotland. It was prepared by 'Syton-polishing' and coated with carbon, prior to imaging at 30 KV accelerating voltage. (a) Orientation contrast image of the deformation microstructure; the different contrasts reflect regions of different crystallographic orientation, whilst the black lines are etched grain boundaries. (b) Selected-area electron channelling pattern (SAECP) from an individual quartz grain; the pattern indicates a crystallographic orientation very close to (0001).

Fig. 2. Examples of ECP-maps for face-centred cubic symmetry constructed from SEM/ECP photomicrographs obtained by tilting a copper single crystal sphere about a fixed point of incidence of the electron beam. (a) Planar ECP-map in which the size of the constituent ECP's has been adjusted to compensate for the distortions which occur with increasing angular distance from the centre of the map at (001). (b) Spherical ECP-map in which the size of constituent ECP's is constant and fixed by the diameter of the sphere; note the curved rulers used to measure the Euler angles.

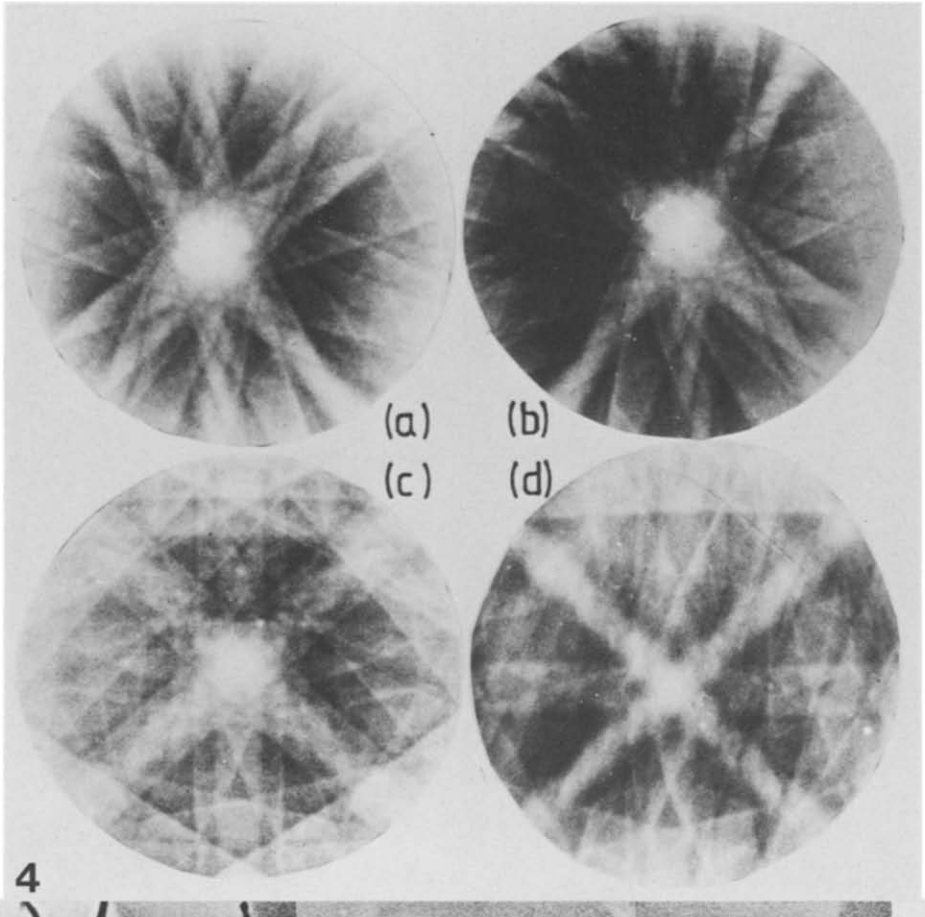

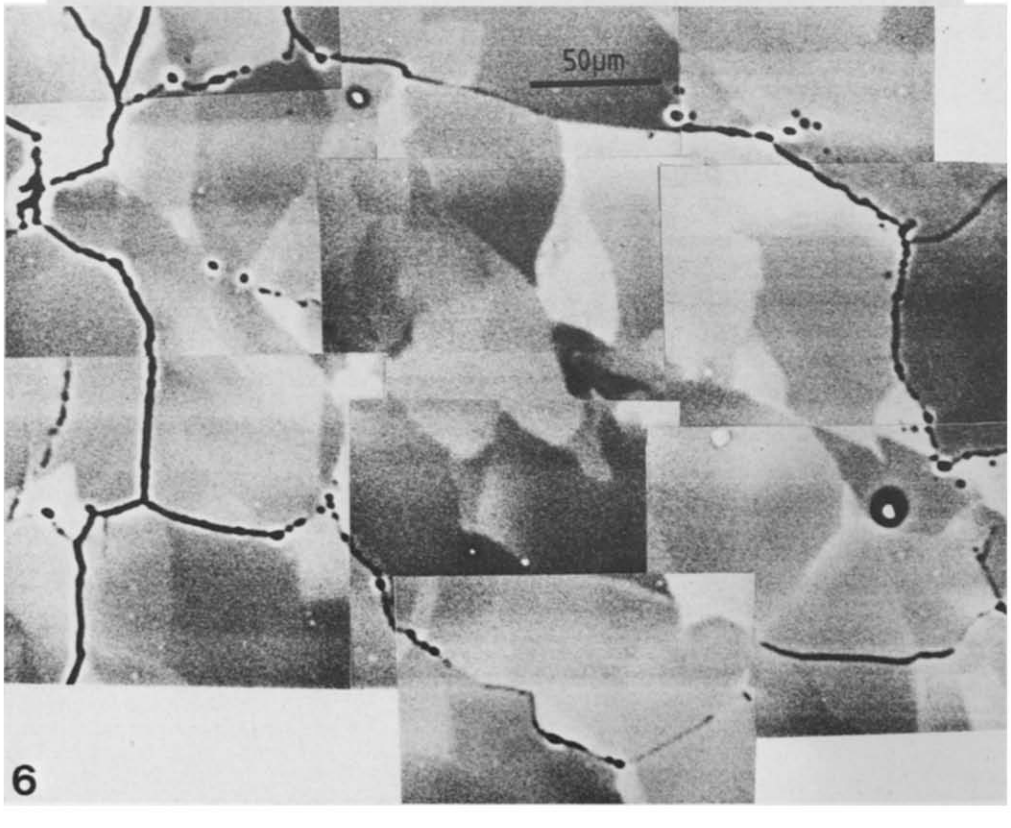

Fig. 4. Distinction between similar crystal forms as shown by their ECP's. (a) and (b) Positive and negative forms of *a*. (c) and (d) *r* and *z* forms.

Fig. 6. High-magnification orientation-contrast photomicrographic montage of an individual quartz grain within the Tongue quartzite (see Fig. 1a) showing the subgrain microstructure in detail.

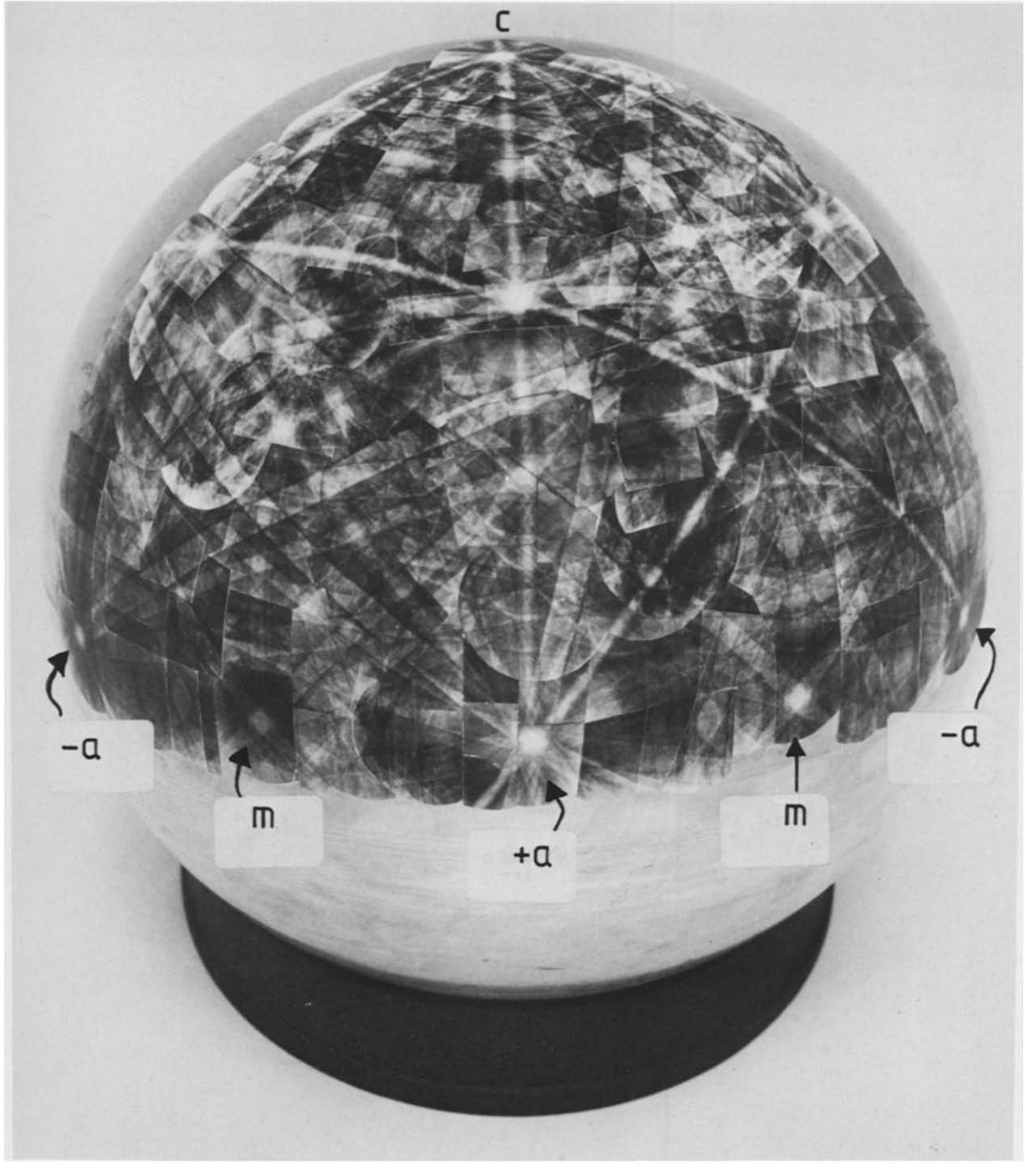

Fig. 5. Spherical ECP-map for quartz covering 120°, or one sixth of the surface of a sphere.

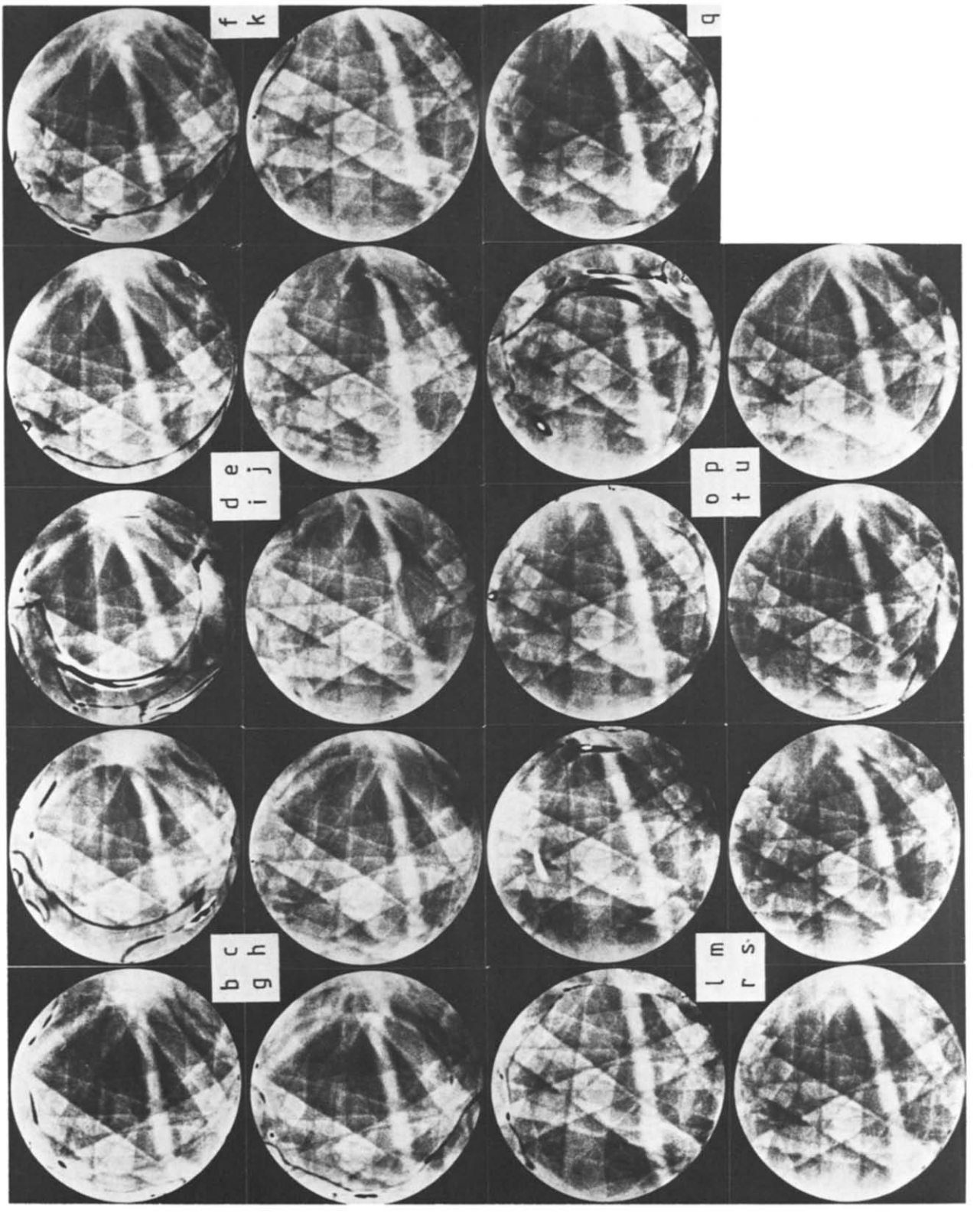

Fig. 7. ECP's from the subgrains shown in Fig. 6 and Table 1; note the general similarity in position of the channelling bands.

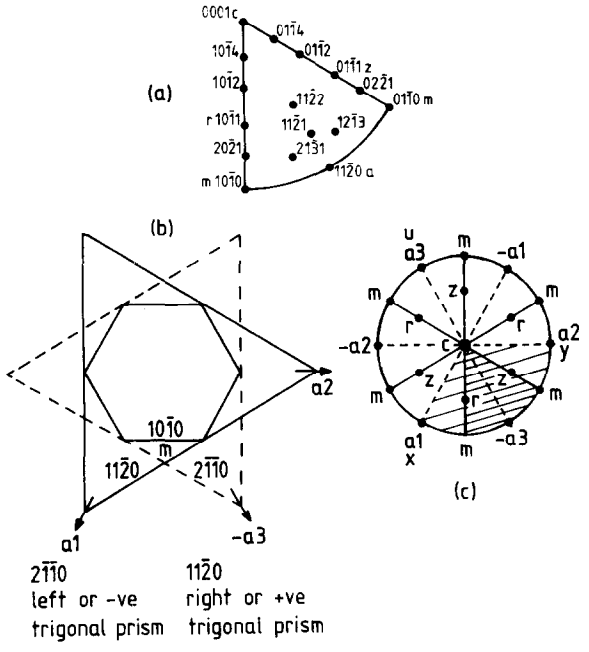

Fig. 3. Crystallographic and stereographic considerations of ECP analysis. (a) Crystallographic unit triangle used in quartz petrofabric studies via the optical microscope and the X-ray texture goniometer; the orientation diagram is an inverse pole figure. (b) Origin of triad symmetry due to the presence of two *a* forms; compare the hexagonal symmetry of the *m* forms. (c) The complete crystallographic stereogram for quartz showing the main forms and their relationships, plus the 60 and 120° unit triangles involved in conventional and ECP analytical procedures.

including a single *a* form (Fig. 3a). However, although the six *m* forms are all identical first-order hexagonal prisms, the six *a* axes are not identical, but consist of three right-handed and three left-handed second-order trigonal prisms (Fig. 3b) which together define a single triad axis of characteristic trigonal symmetry. The two types of *a* are indistinguishable with the X-ray texture goniometer allowing a pseudo-hexagonal 60° unit triangle to be used. In contrast, ECP's clearly reveal the different *a* forms (Figs. 4a & b) and consequently it is impractical to index either form using an ECP-map containing only a single *a*. Unfortunately a 60° unit triangle ECP-map which includes both *a* forms, such as $a_1, c, -a_3$ (e.g. Fig. 3c), also does not contain all possible ECP's since the *r* and *z* forms are clearly distinguishable (Figs. 4c & d).

In order to include all possible ECP configurations, it appears that the quartz ECP-map must extend over a 120° unit triangle containing both *a* forms. The most appropriate construction extends between a_1, *c*, a_2 and includes the conventional 60° unit triangle as the central part of the map (Fig. 3c). An interesting feature of this map is that it contains two planes of partial symmetry (i.e. the zones containing *m* and *c*) such that it is possible to wrap the outer portions into the central 60° triangle. This should make the comparison between inverse pole figures constructed by ECP and optical or X-ray techniques relatively straightforward.

Specimen preparation

A 120° quartz ECP-map is extremely large and covers one third of a hemisphere. It is impossible to construct such a map by tilting a single specimen in the SEM. A large single crystal of Brazilian hydrothermal vein quartz was therefore cut at different orientations to produce 33 specimens. The individual specimens were then used to provide a part of the total ECP-map. A problem with any ECP analysis is that the intensity of the electron-channelling and signal is dependent on the state of the specimen surface, in particular the degree of structural damage (either natural or induced) and the topography. Unfortunately the cutting of the specimens introduces sufficient surface damage to destroy all trace of the ECP's. This damage cannot be adequately removed by conventional polishing techniques involving abrasive powders and pastes, even though these may produce an acceptably smooth surface. Subsequent polishing is necessary using a colloidal silica sol slurry (Syton) and a polyurethane-foam lapping surface.

Having polished the quartz to remove surface damage, it is necessary to coat the specimens with a conducting medium to prevent charging since this degrades the ECP signal as well. A layer of amorphous carbon is deposited onto the specimen by vacuum evaporation, care being taken to minimize the thickness, since too much will also degrade the emitted signal. Details of these specimen preparation procedures are given in Lloyd *et al.* (1981); for a fuller discussion the reader is referred to Lloyd (1985).

SEM operating conditions

The ECP images were obtained using a Cambridge Stereoscan 4 SEM operated in the selected-area diffraction mode and fitted with a semiconductor BSE detector (see Hall & Lloyd 1981, 1983, Lloyd *et al.* 1981 or Lloyd 1985, for full details). Because the 33 quartz specimens were examined separately it was necessary to maintain as far as possible the same operating conditions. This is achieved by using a constant working-distance (i.e. the distance between the specimen and the final SEM lens) obtained by adjusting the final lens control in combination with the specimen-stage height control. A working-distance of 6 mm was used throughout with a constant accelerating voltage of 30 kV.

Each specimen was positioned in the SEM such that initially the electron beam was normal to the surface. To obtain as large a partial ECP-map as possible, each specimen was tilted about three orthogonal axes (θX, θY and θZ)using the goniometer controls on the specimen stage. The maximum tilt possible with the θX and θY controls did not exceed $\pm 20°$ (and was usually somewhat less), but a full 360° rotation was possible with the θZ control. The partial ECP-maps were constructed by recognizing that the ECP's from each specimen contained several major channelling bands. These bands were made to lie in a vertical sense on the SEM/CRT screen using the θZ control and then, by means of the θX and θY tilts, it was possible to move a small distance (up to 20°) along the bands. A photographic recording was made of the ECP observed after every 2.5° of θX tilt for

each vertical position. In this way it is possible to construct a partial ECP-map with a radius of up to 20°.

Rather than construct the complete map by merging together 33 partial ECP-maps over a spherical surface, the ECP photographs were fitted together separately on a metal globe, beginning at the basal plane and working upwards to the *c*-axis. This approach was chosen because even the partial maps contain some distortion due to construction over a plane. By considering the photographs individually, the maximum distortion involved is that included in the photograph. This can be reduced still further by using only the central portion of each photograph. The completed spherical ECP-map for quartz is shown in Fig. 5. A simple example of the use of this map is given in the next section.

USE OF QUARTZ ECP-MAP

As an example of the use of the spherical quartz ECP-map in petrofabric analysis we consider a quartzite from the Tongue region (Grid Reference NC 575643) of northern Scotland, which lies 7.5 km to the east of the Moine Thrust Zone. Deformation in this region is associated with amphibolite facies metamorphism (R. D. Law pers. comm. 1984). The specimen is part of a quartz rod (Wilson 1953) and contains a strong stretching lineation which is parallel to the rodding and also to local fold axes. Figure 1(a) shows a low-magnification SEM orientation contrast photomicrograph of the *XZ* section (i.e. normal to foliation, parallel to lineation) of this specimen; note the subgrain structure present in many of the grains. It should be remembered that the variation in contrast intensity in no way reflects the magnitude of the misorientation; adjacent subgrains with respectively black and white contrasts may be only very slightly misorientated. The intragranular variations in orientation can be determined via ECP analysis.

Figure 6 is a high-magnification orientation-contrast montage of the grain at the centre of Fig. 1(a). The grain contains a considerable number of subgrains, some of which are below the resolution limit for ECP-analysis, although improved imaging techniques such as spiral scanning (e.g. Hall & Skinner 1978) may reveal recognisable ECP's from these smaller subgrains. ECP's have been obtained from as many of the subgrains as possible and are shown in Fig. 7 (see also Fig. 9a for their locations). As might be expected, the individual patterns are similar in appearance, which suggests that only slight misorientations exist within the grain. These misorientations can be determined by indexing the patterns using the spherical ECP-map, as follows. The position of each ECP, as defined by the normal to the centre of the pattern, is recognized by direct visual comparison with the ECP-map and can be fixed within the reference frame of the map by two spherical angles (θ and ϕ) defined in Fig. 8(a). Since the normal to the ECP is also the grain (or subgrain) normal, this approach plots a specimen reference axis (in this case the *Y* direction) in terms of crystal axes and hence produces an inverse pole

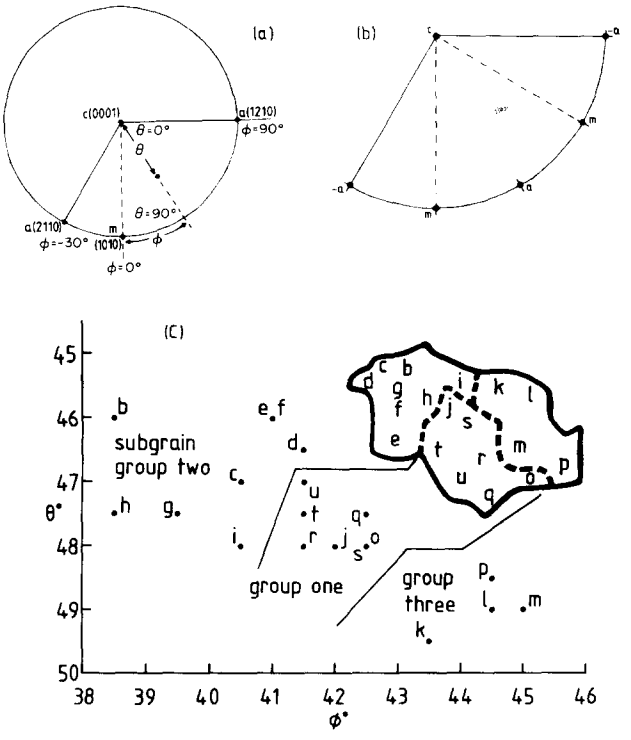

Fig. 8. Results of the analysis of the subgrain fabric in the grain of Tongue quartzite shown in Fig. 6. (a) Definition of the spherical angles θ and ϕ used to constrain the position of the ECP's within the spherical ECP-map. (b) Inverse pole figure of the subgrain orientations. (c) Enlargement of the inverse pole figure in the region of the subgrain orientations to show the relationship between the different subgrains, as labelled in Fig. 7 and Table 1.

figure of the subgrain orientations (Fig. 8b); see also Table 1.

The misorientations between subgrains are small, so they are not clearly revealed using the whole 120° stereogram. However, if the region of the subgrain orientations is enlarged, three distinct groups can be recognised (Fig. 8c): Group One is a tight cluster of orientations situated between Groups Two and Three. The orientation groups also correspond to distinct spatial sub-areas

Table 1. Values of θ and ϕ for each subgrain measured from the positions of their ECP's on a spherical ECP-map. Also listed are the deviations (Δ) from an assumed initial orientation $\theta = 47.7°$, $\phi = 42.1°$ estimated from the 'Group One' subgrains (*)

Subgrain	θ	ϕ	Δ
b	46.0	38.5	3.98
c	47.0	40.5	1.75
d	46.5	41.5	1.34
e	46.0	41.0	2.02
f	46.0	41.0	2.02
g	47.5	39.5	3.11
h	47.5	38.5	3.61
i	48.0	40.5	1.63
j*	48.0	42.0	−0.32
k	49.5	43.5	−2.28
l	49.0	44.5	−2.73
m	49.0	45.0	−3.18
o*	48.0	42.5	−0.50
p	48.5	44.5	−2.53
q*	47.5	42.5	0.45
r*	48.0	41.5	−0.67
s*	48.0	42.5	−0.50
t*	47.5	41.5	0.78
u*	47.0	42.0	0.71

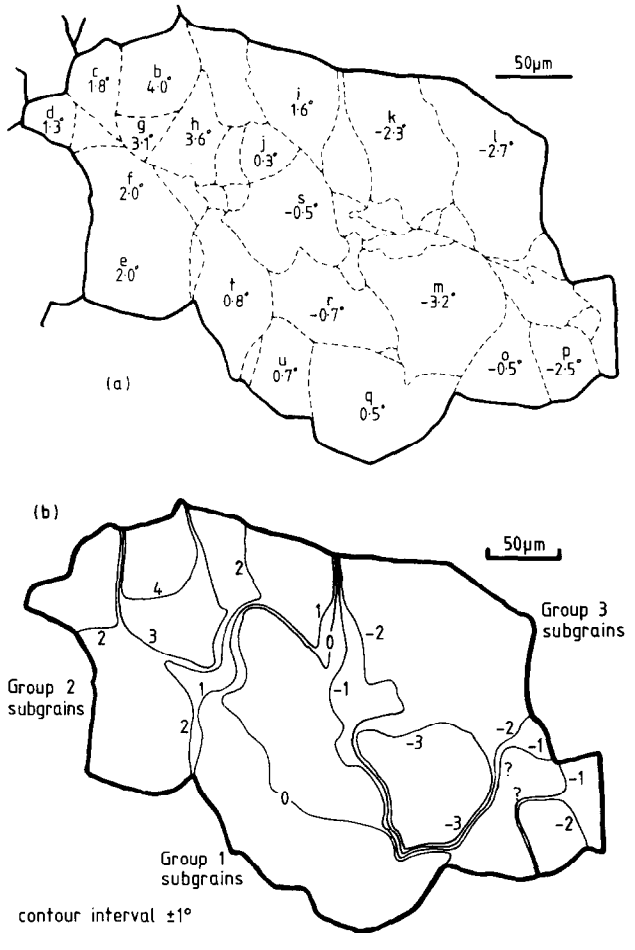

Fig. 9. (a) Distribution of subgrain misorientations determined relative to an assumed original grain orientation. (b) Misorientation contours drawn along subgrain boundaries.

of the grain with Group One occupying the central part of the grain between the other two (Fig. 8c). The relative misorientation of subgrains within Group One is much less than in the other two groups and it is probable that Groups Two and Three have evolved from Group One. The misorientation of the subgrains (Δ) can therefore be considered in terms of an original orientation, which we take to be close to the Group One orientations, and which we estimate from the statistical means of the θ and ϕ values of the Group One subgrains (Table 1).

The deviation of subgrains from the estimated original orientation is shown diagramatically in Fig. 9(a). Since the crystal structure deformations responsible for the misorientations are generally accommodated in the subgrain walls, misorientation contours can be drawn between the subgrains depending on their particular deviation (Fig. 9b). Note that the misorientation does not develop evenly across the grain, but is concentrated in certain subgrain boundaries such that the grain is essentially composed of three large subgrains (i.e. Groups One, Two and Three) each of which possesses its own 'subgrain' structure.

Although our study of this specimen was initiated mainly to illustrate the use of the ECP-map, it is a measure of the technique's potential value that the results have important tectonic implications. There is growing experimental evidence that the size of new grains or subgrains developing during dynamic recrystallization is a function of the local stresses (Mercier *et al.* 1977, Twiss 1977, Ross *et al.* 1980). In spite of the many uncertainties (discussed by White 1979), grain-size–stress relations derived from laboratory experiments are used increasingly to derive palaeostress estimates (Nicholas 1978, Mercier 1980, Kohlstedt & Weathers 1980, Christie & Ord 1980, Etheridge & Wilkie 1981, White 1982). Most of the relevant experimental work relates to recrystallization by grain-boundary migration, a relatively high temperature phenomenon characterized by bulging and suturing of grain boundaries. These features are not apparent in our example; the incipient recrystallization appears to be by subgrain rotation, a process usually characterized by the development of new grains having the same grain size as the precursor subgrains. When subgrains are found within new grains this is often taken to imply a new wave of deformation in response to increasing applied stress. However our work clearly demonstrates that small subgrains are already developed before large subgrains (i.e. Groups One, Two and Three) are sufficiently misorientated to be described as new grains. TEM observations often reveal subgrains on a still smaller scale and it seems likely that hierarchical arrangements of subgrains within subgrains, perhaps spanning two orders of magnitude in size, can develop concurrently. This casts severe doubt on the existence of any simple relationship between grain size and applied stress during rotational crystallization.

CONCLUSIONS

SEM electron channelling has the potential to become an important method for microstructural analysis, rivalling conventional U-stage microscopy and the newer technique of X-ray texture goniometry. It is therefore pertinent to reiterate the advantages of the method.

(1) Electron channelling is completely discriminatory in that the spatial and orientation information on grains are always in one-to-one correspondence.

(2) The technique is equally applicable to monomineralic and polymineralic rocks.

(3) The minimum grain size possible for *useful* ECP resolution is typically >10μm, but refined SEM electro-optics can reduce this to >1μm. However, deformed and/or fine grains often yield distorted ECP's unsuitable for interpretation.

(4) All crystallographic orientations can be recognised and complete textural descriptions in the form of orientation distribution function diagrams can be obtained without the need for complex mathematical functions. Pole figures and inverse pole figures are also easily obtainable.

(5) Orientation-contrast images are typically resolvable to magnifications in excess of 1000 times normal.

The principal disadvantage of the electron-channelling technique is that it is essentially manual and therefore tends to be slow and tedious. This is a drawback

only for bulk fabric analyses in which, for statistical validity, somewhere in excess of 500 ECP's need to be individually imaged, photographed and indexed. However, for studies of localized fabrics and microstructures the effort required is negligible compared to the potential rewards.

The work described in this paper represents the basis for future studies of microstructures and petrofabrics in quartz rocks using the SEM electron-channelling technique. The standard SEM methodology and spherical map for indexing are now available, and more applications will no doubt lead to further refinements of both technique and interpretation. As a first step, bulk fabric determinations of quartz rocks using ECP's are essential so that the fabrics can be compared with those derived via optical and/or X-ray techniques. We are currently engaged in a bulk fabric determination of the Tongue quartzite for this purpose.

Acknowledgements—This work was supported by NERC Grant GR3/4461. We thank Rick Law for the specimen of Tongue quartzite and for his comments on the manuscript. Sue Dipple and Mark Dallas are also thanked for technical assistance with the scanning electron microscopy, while Dave Finch helped prepare the ECP photographs. We are also grateful to our referees for their perceptive comments.

REFERENCES

Booker, G. R., Shaw, A. M. B., Whelan, M. J. & Hirsch, P. B. 1967. Some comments on the interpretation of the 'Kikuchi-like reflection patterns' observed by scanning electron microscopy. *Phil. Mag.* **16**, 1185–1191.

Bunge, H. J. & Wenk, H. R., 1977. Three-dimensional texture analysis of three quartzites (trigonal crystal and triclinic specimen symmetry). *Tectonophysics* **40**, 257–285.

Christie, J. M. & Ord, A. 1980. Flow stresses from microstructures of mylonites: examples and current assessment. *J. geophys. Res.* **85**, 6253–6262.

Etheridge, M. A. & Wilkie, J. C. 1981. An assessment of dynamically recrystallised grain size as a palaeopiezometer in quartz-bearing mylonite zones. *Tectonophysics* **78**, 475–508.

Goldstein, J. I. & Yakowitz, H. 1975. *Practical Scanning Electron Microscopy*. Plenum, New York.

Hall, M. G. & Hutchinson, W. B. 1980. Smooth surface metallography using the scanning electron microscope. *Metall. Mater. Technol.* **12**, 371–375.

Hall, M. G. & Lloyd, G. E., 1981. The SEM examination of geological samples with a semiconductor backscattered electron detector. *Am. Miner.* **66**, 362–368.

Hall, M. G. & Lloyd, G. E. 1983. The SEM examination of geological samples with semiconductor backscattered electron detector: reply. *Am. Miner.* **68**, 843–845.

Hall, M. G. & Skinner, G. K. 1978. A spiral scanning attachment for electron channelling studies with a scanning electron microscope. *J. Phys. E* **11**, 1129–1132.

Hirsch, P. B., Howie, A. & Whelan, M. J. 1962. On the production of X-rays in thin metal foils. *Phil. Mag.* **7**, 2095–2100.

Holt, D. B., Muir, M. D., Boswarva, I. M. & Grant, P. R. 1974 (Editors). *Quantitative Scanning Electron Microscopy*. Academic Press, New York.

Joy, D. C., 1974. Electron channelling patterns in the scanning electron microscope. In: *Quantitative Scanning Electron Microscopy* (edited by D. B. Holt, M. D. Muir, I. M. Boswarva and P. R. Grant). Academic Press, New York.

Kohlstedt, D. L. & Weathers, M. S. 1980. Deformation-induced microstructures, palaeopiezometers, and differential stress in deeply eroded fault zones. *J. geophys. Res.* **85**, 6269–6285.

Lloyd, G. E. 1985. Review of instrumentation, techniques and applications of SEM in mineralogy. In: *Applications of Electron Microscopy in the Earth Sciences* (edited by J. C. White). Mineralogical Association of Canada Short Course **11**, 151–188.

Lloyd, G. E. & Hall, M. G. 1981. Application of scanning electron microscopy to the study of deformed rocks. *Tectonophysics* **78**, 687–698.

Lloyd, G. E., Hall, M. G. Cockayne, B. & Jones, D. W. 1981. Selected area electron-channelling patterns from geological materials: specimen preparation, indexing and representation of patterns and applications. *Can. Mineralogist* **19**, 505–518.

Mercier, J.-C. 1980. Magnitude of the continental lithospheric stresses inferred from rheomorphic petrology. *J. geophys. Res.* **85**, 6293–6303.

Mercier, J.-C., Anderson, D. A. & Carter, N. L. 1977. Stress in the lithosphere: inferences from steady-state flow of rocks. *Pure appl. Geophys.* **115**, 199–226.

Nicolas, A. 1978. Stress estimates from structural studies in some mantle peridotites. *Phil. Trans. R. Soc.* **A288**, 49–57.

Roe, R. J. 1965. Descriptions of crystallite orientation in polycrystalline materials—III. General solution to pole figure inversion. *J. appl. Phys.* **36**, 2024–2031.

Ross, J. V., Avé Lallement, H. G. & Carter, N. L. 1980. Stress dependence of recrystallised-grain size in olivine. *Tectonophysics* **70**, 39–61.

Saimoto, S., Helmstaedt, H., Kempson, D. & Schulson, E. M. 1980. Electron channelling and its potential for petrofabric studies. *Can. Mineralogist* **18**, 251–259.

Schulson, E. M. 1977. Electron channelling patterns in scanning electron microscopy. *J. Mater. Sci.* **12**, 1071–1087.

Stott, D. E., Wise, M. L. H. & Hutchinson, W. B. 1975. A distortion-free map for use with electron channelling patterns. *J. Micros.* **105**, 305–307.

Twiss, R. J. 1977. Theory and applicability of a recrystallised grain size palaeopiezometer. *Pure appl. Geophys.* **115**, 227–244.

White, J. C. 1982. Quartz deformation and the recognition of recrystallisation regimes in the Flinton Group conglomerates, Ontario. *Can. J. Earth Sci.* **19**, 81–93.

White, S. 1979. Difficulties associated with palaeostress estimates. *Bull. Mineral.* **102**, 210–215.

Williams, R. O. 1968. The representation of the textures of rolled copper, brass and aluminium by biaxial pole figures. *Trans. Metall. Soc. A.I.M.E.* **242**, 105–115.

Wilson, G. 1953. Mullion and rodding structures in the Moine series of Scotland. *Proc. geol. Ass.* **64**, 118.